DETC2019-97934

MULTIMATERIAL TOPOLOGY OPTIMIZATION OF THERMOELECTRIC GENERATORS

Xiaoqiang Xu1

¹Department of Mechanical Engineering State University of New York at Stony Brook Stony Brook, NY 11794, USA Email:Xiaogiang.Xu@stonybrook.edu

Lei Zuo²

²Department of Mechanical Engineering Virginia Tech Blacksburg, VA 24060, USA Email: Leizuo@vt.edu

Yongjia Wu²

²Department of Mechanical Engineering Virginia Tech Blacksburg, VA 24060, USA Email: Yjwu2015@vt.edu

Shikui Chen^{1,*}

¹Department of Mechanical Engineering State University of New York at Stony Brook Stony Brook, NY 11794, USA Email: shikui.chen@stonybrook.edu

ABSTRACT

Over 50% of the energy from power plants, vehicles, oil refining, and steel or glass making process is released to the atmosphere as waste heat. As an attempt to deal with the growing energy crisis, the solid-state thermoelectric generator (TEG), which converts the waste heat into electricity using Seebeck phenomenon, has gained increasing popularity. Since the figures of merit of the thermoelectric materials are temperature dependent, it is not feasible to achieve high efficiency of the thermoelectric conversion using only one single thermoelectric material in a wide temperature range. To address this challenge, this paper proposes a method based on topology optimization to optimize the layouts of functional graded TEGs consisting of multiple materials. The objective of the optimization problem is to maximize the output power and conversion efficiency as well. The proposed method is implemented using the Solid Isotropic Material with Penalization (SIMP) method. The proposed method can make the most of the potential of different thermoelectric materials by distributing each material into its optimal working temperature interval. Instead of dummy materials, both the P and N-type electric conductors are optimally distributed with two different practical thermoelectric materials, namely Bi_2Te_3 & PbTe for P-type, and Bi_2Te_3 & $CoSb_3$ for N-type respectively, with the yielding conversion efficiency around 12.5% in the temperature range T_c =25°C and T_h =400°C. In the 2.5D computational simulation, however, the conversion efficiency shows a significant drop. This could be attributed to the mismatch of the external load and internal TEG resistance as well as the grey region from the topology optimization results as discussed in this paper.

1 INTRODUCTION

Since its discovery, the thermoelectric effect, which can convert temperature differences into the electric voltage and vice versa, has aroused a lot of interests among researchers, especially in such an energy sustainable society. One important application of such effect is the thermoelectric generator (TEG), which can transform a tremendous amount of waste heat generated from various sources like home heating, automotive exhaust, and industrial processes into electricity [1]. Such devices occupy unique advantages over other thermal power-generation devices.

^{*}Address all correspondence to this author.

For example, it can be designed in flexible size, operate without moving parts thus quite reliable, and very environmentally friendly [2]. However, one major weakness is that the efficiency of a TEG has been relatively low, which, to a certain extent, impedes the broader application of such technology into various fields.

Typically, besides the temperature difference between the hot and cold end, the efficiency of a TEG relies heavily on the figure of merit of the thermoelectric material, $zT = \alpha^2 T/\rho \kappa$, where T is absolute temperature, α is the Seebeck coefficient, ρ is the electrical resistivity and κ is the thermal conductivity, respectively [3]. Over the past several decades, tremendous effort has been made to enhance the zT value of the thermoelectric materials. For example, several breakthroughs have been made in the nanoscale from the standpoint of materials science, such as the all-scale hierarchical architectures to reduce the thermal conductivity [4], preparing thermoelectric materials like Bi₂Te₃ in quantum-well super-lattice structures [5] and band engineering [6, 7] to increase the power factor (α^2/ρ) . Due to these advances, the figure of merit of the TE materials could reach 1.8 with the corresponding conversion efficiency increasing to 11%-15% [2].

In addition to the progress from the material science perspective, researchers from the mechanical engineering community also contribute by exploring the full potential of the existing thermoelectric materials. One typical example is the segmented thermoelectric generator [8], in which the P and N-type elements are usually divided into several segments. In each segment, a proper thermoelectric material is employed to achieve the highest efficiency in the temperature interval of that segment. For simple regular geometry, it is convenient to determine the dimensions for each segment. But it is difficult to treat with a TEG with complex and irregular geometry. Therefore, in this paper, we propose a new method based on topology optimization to find the optimal thermoelectric materials distribution to achieve the highest conversion efficiency.

Topology optimization has emerged for nearly 30 years since its introduction by MP Bendse and N Kikuchi in 1988 [9], which aims at finding the proper materials layout in a prescribed domain to obtain the best performance for a certain purpose. One outstanding characteristic of topology optimization lies in that it can give you designs independent on your initial guess. Several major topology optimization approaches have been proposed over the years, including SIMP (Solid Isotropic Material Penalization) [10, 11], level set method [12, 13], phase field [14] and topological derivative [15]. In this paper, SIMP is employed since it is quite straightforward. To implement the SIMP, several relationships between the density variable and the thermoelectric properties need to be established. And to make it more accurate, the temperature-dependence of the thermoelectric materials properties are taken into consideration in the form of cubic spline interpolation functions. The output power and conversion efficiency are treated as the objectives to be optimized.

This paper is organized as follows: in Section 2, the governing equations for thermoelectric phenomena are introduced. The topology optimization formulation is given in Section 3, including computational model description, objective functions and material interpolation scheme. Section 4 details the numerical implementation, followed by the topology optimization results and 2.5D numerical verification in Section 5. Finally, in Section 6, the results are discussed, and some concluding remarks are given.

2 THERMOELECTRIC GOVERNING EQUATIONS

A typical TEG is shown in Figure 1, which usually consists of heat source, heat sink, P and N-type thermoelectric elements, external load, and electrodes (gray regions). It works based on the Seebeck effect, where an electromotive force is built due to the movement of charge carriers in the presence of a temperature gradient between the hot and cold ends. When connected to an external load to build a circuit, there will be a current flowing through to produce electric power. For P-type, the current is carried by holes, while for N-type, it is by electrons. We can imagine the potential application of such a TEG device wherever there is a temperature gradient.

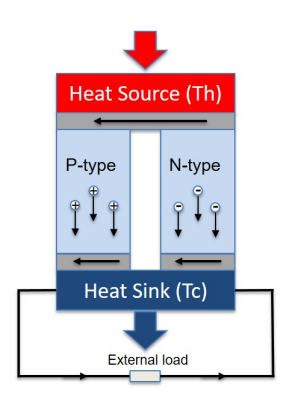


FIGURE 1: The configuration of a typical TEG device

This multi-physics optimization problem involves heat transfer in solids, electron migration, and thermoelectric effect. For simplicity, we only consider the steady state and assume that the thermoelectric materials are isotropic with regards to the thermoelectric properties like Seebeck coefficient, electrical conductivity, and thermal conductivity. Consulting [16, 17], the governing equations for electrical and thermal conductions can be given as follows:

$$\nabla \cdot \boldsymbol{J} = 0 \tag{1}$$

$$\nabla \cdot \boldsymbol{q} = f \tag{2}$$

The above equation (1) and (2) are coupled with the following thermoelectric constitutive equations:

$$\boldsymbol{J} = \boldsymbol{\sigma}(\boldsymbol{E} - \boldsymbol{\alpha} \nabla T) \tag{3}$$

$$q = \beta J - \kappa \nabla T \tag{4}$$

where:

J = electric current density vector, A/m²,

q = heat flux density vector, W/m²,

 $f = \mathbf{J} \cdot \mathbf{E}$ is the heat generation rate per unit volume, W/m³,

 σ = electric conductivity, S/m,

 $E = -\nabla V$, electric field intensity vector, V/m; V is electric potential, V,

 α = Seebeck coefficient, V/K,

T = absolute temperature field, K,

 $\beta = T \cdot \alpha$ denotes the Peltier coefficient, V,

 κ = thermal conductivity, W/(m·K).

The boundary conditions are:

$$V = V_0$$
, fixed electric potential (5a)

$$T = T_c$$
, fixed temperature (5b)

$$T = T_h$$
, fixed temperature (5c)

$$\mathbf{n} \cdot \mathbf{J} = 0$$
, electrical insulation (5d)

$$\mathbf{n} \cdot \mathbf{q} = 0$$
, thermal insulation (5e)

By imposing the above boundary conditions, the equation (1) and (2) can be solved with respect to the two state variables T and V, which will be further used to compute the objective functions and constraints.

3 TOPOLOGY OPTIMIZATION FORMULATION

Topology optimization has been a robust tool for finding the optimal materials layout for a particular purpose. In this paper, different thermoelectric materials are to be optimally distributed in the P & N-type thermoelectric elements, i.e., the design domain. For simplicity, in the topology optimization stage, only 2D problem is considered.

3.1 Computational model description

As seen in Figure 2, a 2D computational model is built. Unlike the conventional configuration in Figure 1, this model adopts

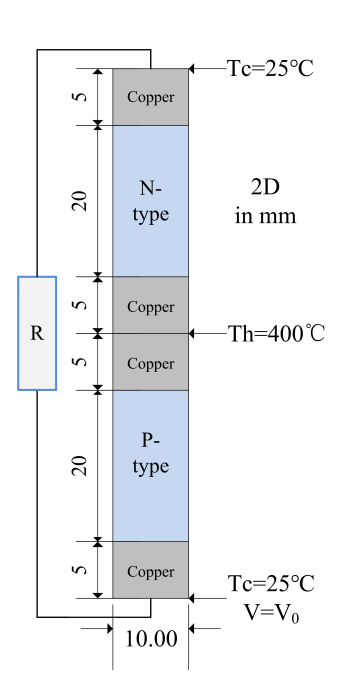


FIGURE 2: Diagram of the computational model

a stack junction, which could reduce the parasitic losses from the connection between the P and N-type electrical conductors [18]. The thickness is 1mm to make it a thin plate structure. The temperature for the hot and cold end is set to be $400\,^{\circ}$ C and $25\,^{\circ}$ C respectively. An electrical potential V_0 is assigned to the bottom surface. Copper acts as electrodes. An external load R is connected to form an electrical circuit and produce power. All other outer boundaries of the whole domain are electrically insulated and adiabatic, corresponding to the Neumann boundary conditions in equations (5d) and (5e).

3.2 Objective functions

In this topology optimization problem, we have two objective functions to optimize, namely output power and conversion efficiency. When there is a large amount of heat sources, maximum output power is preferably wanted. While when the heat source is limited, we prefer a maximum conversion efficiency, which is defined as the ratio between output power and the total heat flow from the source. For output power:

$$P_{out} = \int_{\Omega_1} \mathbf{J} \cdot \mathbf{E} d\Omega \tag{6}$$

where J is the electric current density vector; E is the electrical field intensity vector as mentioned earlier; Ω_1 is the external resistor domain.

The conversion efficiency is defined as follows:

$$\eta = \frac{P_{out}}{Q} = \frac{\int_{\Omega_1} \boldsymbol{J} \cdot \boldsymbol{E} d\Omega}{|\int_{\Omega_2} \boldsymbol{q} \ d\Omega|}$$
(7)

where Q is the total heat flow from the source; q is the heat flux density vector; Ω_2 is the domain from which the heat flows in.

Thus, the objective of the topology optimization problem is to maximize either the output power or the conversion efficiency, which can be formulated as follows:

maximize
$$J_1 = P_{out}$$
, (8)

or maximize
$$J_2 = \eta$$
, (9)

subject to:

$$\int_{\Omega_{PN}} dx < V_f \cdot A. \tag{10}$$

In the above equations, Ω_{PN} refers to regions occupied by thermoelectric materials of the final design; V_f is the volume ratio; A is the initial area of the P and N-type elements. In practice, a large number of TEG units would be connected electrically in series and thermally in parallel to produce massive power, requiring a lot of thermoelectric materials. Therefore, it is advisable to impose a volume constraint in the designing process of a TEG unit taking the total cost and weight into consideration.

3.3 Material interpolation scheme

The crux of the SIMP method is that a proper relationship between the design variables and corresponding physical properties must be established. In this paper, both the P and N-type thermoelectric materials are optimized. Following [19], we employ the following material interpolation scheme in this paper:

$$\alpha(\rho_{1}, \rho_{2}) = \rho_{1}^{p}(\rho_{2}^{p}\alpha_{1} + (1 - \rho_{2}^{p})\alpha_{2}),$$

$$\kappa(\rho_{1}, \rho_{2}) = \rho_{1}^{p}(\rho_{2}^{p}\kappa_{1} + (1 - \rho_{2}^{p})\kappa_{2}),$$

$$\sigma(\rho_{1}, \rho_{2}) = \rho_{1}^{p}(\rho_{2}^{p}\sigma_{1} + (1 - \rho_{2}^{p})\sigma_{2}),$$
(11)

where $0 < \rho_1 < 1$, $0 < \rho_2 < 1$; p is the penalty factor and is set to be 3. The symbols α_i , κ_i , σ_i , i = 1, 2 denote the Seebeck coefficient, thermal conductivity and electrical conductivity of the two thermoelectric materials respectively. At each point of the design domain, there are two design variables, where ρ_1 is used to determine whether it is material or void and ρ_2 is used to indicate which material it is.

4 NUMERICAL IMPLEMENTATION

The procedures of the topology optimization process are shown in Figure 3. To perform the numerical implementation, the governing equations must be solved correctly to obtain the state fields, i.e., temperature and electrical potential fields in this case, and further to compute the objective functions and constraints. If it is not converged, sensitivity analysis needs to be conducted and later to update the design variables using the Method of Moving Asymptotes (MMA) algorithm [20] in this paper. Once converged, some post-processing steps, like smoothing the boundary to facilitate the manufacturing process, need to be included before the final design is presented. The above procedures are realized with the Comsol multiphysics FEA software.

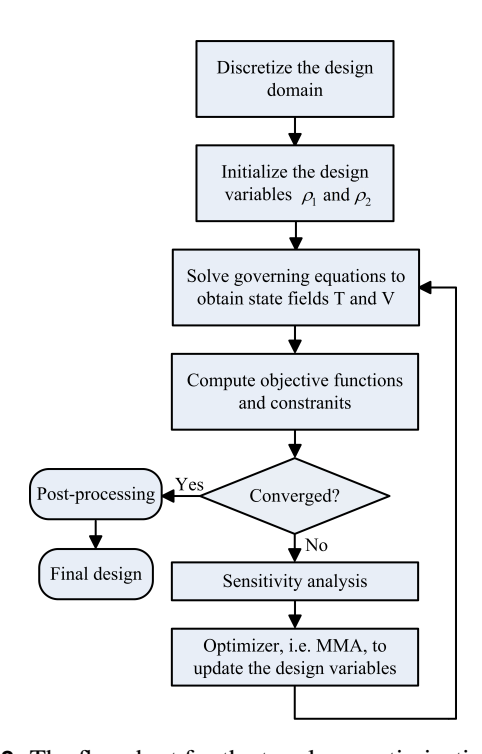


FIGURE 3: The flowchart for the topology optimization process

4.1 Material properties

The properties of the copper electrodes are: $\alpha=6.5\times 10^{-6} \text{V/K}$, $\kappa=400 \text{W/(m*K)}$, $\sigma=5.998\times 10^{7} \text{S/m}$. Because the temperature ranges from T_c =25°C to T_h =400°C, two different thermoelectric materials are employed for each of the P and N-type elements, as shown in Table 1 based on the ZT value from [1]. Such selection makes sure that there are a low-temperature and high-temperature thermoelectric material relatively for each

type element, making it possible to make the most of the thermoelectric capability of each material.

P type	Bi ₂ Te ₃	PbTe
N type	Bi ₂ Te ₃	CoSb ₃

TABLE 1: Material selection

The temperature-dependency of thermoelectric materials properties is taken into account and plotted based on the data from [21,22] in Figure 4.

4.2 Finite element formulation

The governing equations are highly nonlinear due to the coupling of electrical and thermal conductions as well as the strong temperature dependence of the thermoelectric materials properties. They are solved in discretized forms by standard finite element method [23].

$$\begin{bmatrix} \mathbf{K}^{VT} & \mathbf{K}^{VV} \\ \mathbf{K}^{TT} & \mathbf{0} \end{bmatrix} \begin{Bmatrix} \mathbf{T}^{n} \\ \mathbf{V}^{n} \end{Bmatrix} = \begin{Bmatrix} \mathbf{0} \\ \mathbf{Q}^{P} + \mathbf{Q}^{E} \end{Bmatrix}$$
(12)

$$\mathbf{K}^{VT} = \sum_{1}^{n} \int_{\Omega^{e}} [B]^{T} \alpha \sigma[B] d\Omega^{e}$$
 (13a)

$$\mathbf{K}^{VV} = \sum_{1}^{n} \int_{\Omega^{e}} [B]^{T} \sigma[B] d\Omega^{e}$$
 (13b)

$$\mathbf{K}^{TT} = \sum_{1}^{n} \int_{\Omega^{e}} [B]^{T} \lambda [B] d\Omega^{e}$$
 (13c)

$$\mathbf{Q}^{P} = \sum_{1}^{n} \int_{\Omega^{e}} [\mathbf{B}]^{T} \boldsymbol{\beta} [\mathbf{J}] d\Omega^{e}$$
 (13d)

$$\mathbf{Q}^{E} = \sum_{1}^{n} \int_{\Omega^{e}} [N]^{T} [\mathbf{J}]^{T} [\mathbf{E}]^{T} d\Omega^{e}$$
 (13e)

where $\mathbf{T}^n, \mathbf{V}^n$ represent the nodal temperature and nodal electrical potential vector respectively. N is the linear shape function and $B = \nabla N$. The finite element analysis is performed using mapped quadrilateral elements.

The above discretized system is obtained following the general procedures: first multiply the original governing equations with test functions, integrate over the whole domain by parts, and utilize the 2D divergence theorem.

4.3 Sensitivity analysis

The sensitivity information, i.e., the total derivative of objective functions with respect to the design variables, must be derived to update the design in each iteration. In this paper, the adjoint method [24] is employed, which starts from the discretized system as shown in Section 4.2. The equation (12) can be rewritten in the following residual form.

$$\mathbf{R}(\rho, \mathbf{U}) = \mathbf{K}(\rho, \mathbf{U}) \cdot \mathbf{U} - \mathbf{F}(\rho, \mathbf{U}) \tag{14}$$

where \mathbf{R} is the residual vector; \mathbf{K} is the global stiffness matrix; \mathbf{U} is the state variable vector, i.e., $\{\mathbf{T}, \mathbf{V}\}$ in this case and \mathbf{F} is the global load vector.

Then the general Lagrangian function can be formulated as:

$$\mathbf{L}(\rho, \mathbf{U}) = J(\rho, \mathbf{U}) + \lambda^T \cdot \mathbf{R}(\rho, \mathbf{U})$$
 (15)

 λ^T is the Lagragian multiplier. The differentiation of the objective function J in relation to design variable ρ is calculated by:

$$\frac{dJ}{d\rho} = \frac{d\mathbf{L}}{d\rho} = \frac{\partial J}{\partial \rho} + \frac{\partial J}{\partial \mathbf{U}} \cdot \frac{d\mathbf{U}}{d\rho} + \lambda^T \cdot \left[\frac{\partial \mathbf{R}}{\partial \rho} + \frac{\partial \mathbf{R}}{\partial \mathbf{U}} \cdot \frac{d\mathbf{U}}{d\rho} \right]$$
(16)

The crucial point of the adjoint method in conducting sensitivity analysis is to get rid of the derivative of the state variables with respect to the design variables, which can be done by solving the following adjoint equation for proper λ^T :

$$\lambda^T \cdot \frac{\partial \mathbf{R}}{\partial \mathbf{U}} = -\frac{\partial J}{\partial \mathbf{U}} \tag{17}$$

Once λ^T is obtained, we can get the sensitivity information from equation (16).

5 PRELIMINARY RESULTS

5.1 Topology optimization results

The following topology optimization results in Figure 5 are obtained by setting the volume ratio $V_f = 0.6$ and the external load $R = 0.1\Omega$. The initial design is given such that $\rho_1 = V_f$ and $\rho_2 = 1$. With reference to Figure 4(d), the results make sense in that the relatively high-temperature thermoelectric materials PbTe and CoSb₃ are distributed near the hot end, while the relatively low-temperature thermoelectric materials Bi₂Te₃ near the cold end. In other words, each thermoelectric material is placed

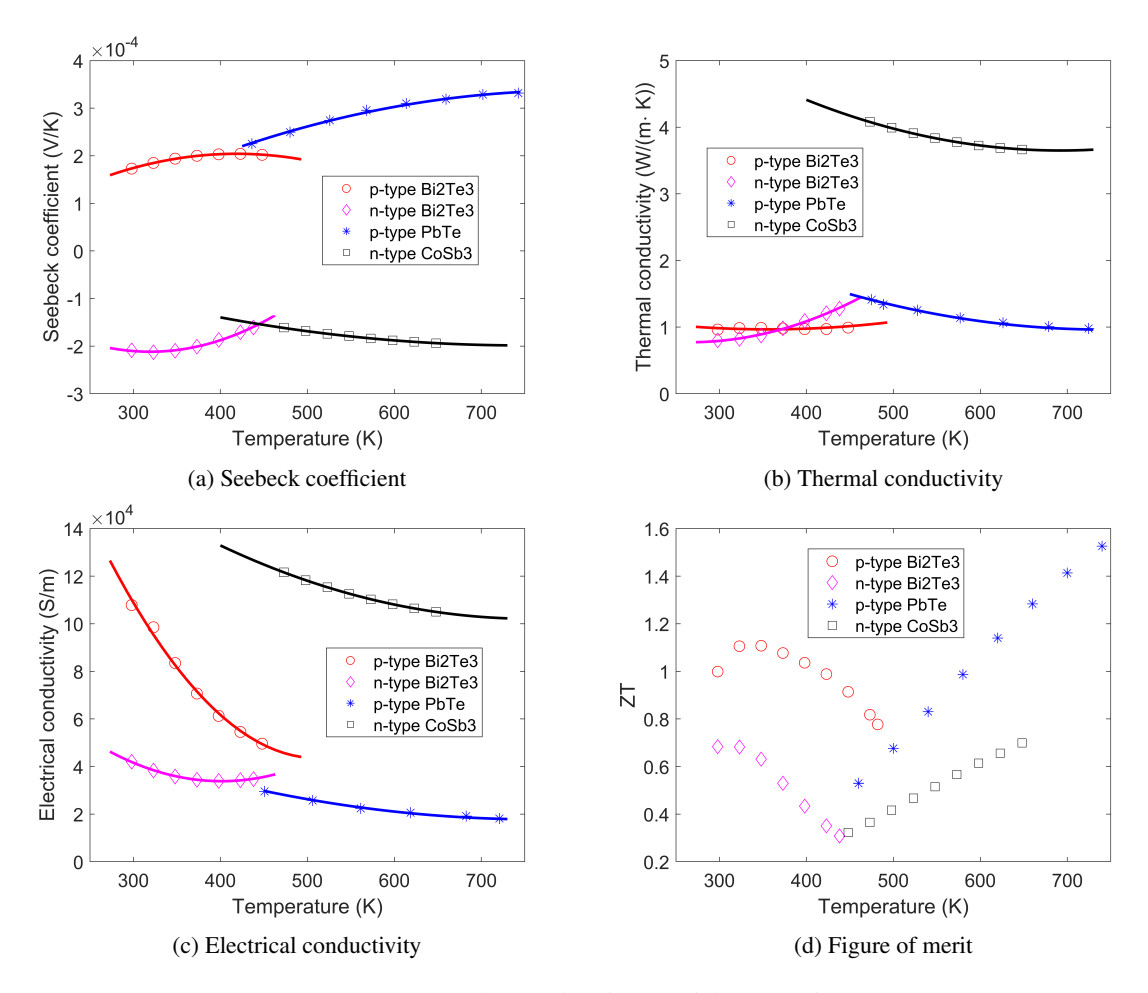


FIGURE 4: Thermoelectric materials properties

into its optimal working temperature interval to fully exploit their thermoelectric capability. The conversion efficiency could reach 12.4%.

The convergence curves for conversion efficiency and output power are shown in Figure 6. As expected, both objectives improve significantly compared with the initial designs.

By tuning the volume ratio V_f from 1 to 0.4, we can obtain a series of optimized TEG structure as shown in Figure 7 and Figure 8. The highest conversion efficiency of 4 different volume ratio cases could reach 13.24%. It is noticeable from Figure 8a and 8b that although the initial volume ratio V_f is given as 1 and 0.8, the actual volume ratio of the final design is 0.936 and 0.745 respectively. This means that in terms of conversion efficiency, it is not the more thermoelectric materials, the higher conversion efficiency.

5.2 Numerical Verification

In this section, a 2.5D model is built and simulated based on the optimized TEG structures obtained from the topology optimization algorithm proposed in this paper. As shown in Figure 9 and Figure 10, two prototypes are built corresponding to the results for both output power and conversion efficiency as the objective function with the volume ration $V_f = 0.6$. The overall dimensions of these two models are $60 \times 10 \times 1$ mm, which is in consistence with the 2D geometry with a thickness of 1mm as described in Section 3.1. The same boundary conditions are applied as in Figure 2. That is: the two end surfaces of copper are assigned low temperature with $T_c=25$ °C, and the middle plane of the central copper electrode is treated as the hot end with T_h =400 °C. A zero electrical potential is placed on the lower end copper surface. And all other surfaces of the domain are prescribed as adiabatic and electrically insulated boundaries. The external resistor is still set to be $R = 0.1\Omega$.

The temperature and electrical potential distribution of the two simulated models are shown in Figure 11, 12, 13 and 14 re-

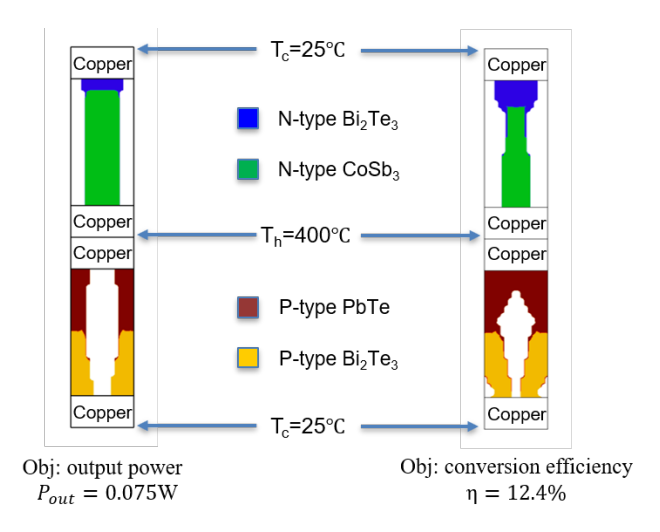


FIGURE 5: Topology optimization results for $V_f = 0.6$

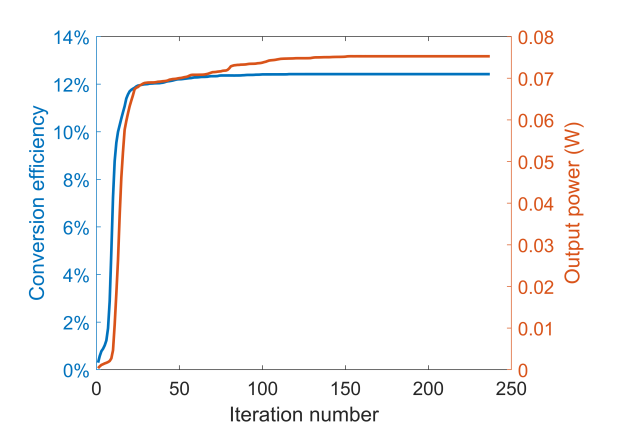


FIGURE 6: Convergence history for $V_f = 0.6$

spectively. It is worth noticing, however, that the simulated output power $P_{out}=0.036\mathrm{W}$ and conversion efficiency $\eta=7.30\%$ are quite smaller than those from the topology optimization results. The causes of these discrepancies will be discussed in details in Section 6.

6 DISCUSSION AND FUTURE WORK

In this paper, a SIMP-based topology optimization method is applied to the thermoelectric problems with the aim of maximizing the output power and conversion efficiency by optimizing the layouts of different thermoelectric materials in a prescribed domain. With the external load fixed at $R=0.1\Omega$, the highest output power and conversion efficiency could reach 0.075W and 12.42% respectively for $V_f=0.6$, which is quite promising compared with the results from [8]. However, these two indexes ob-

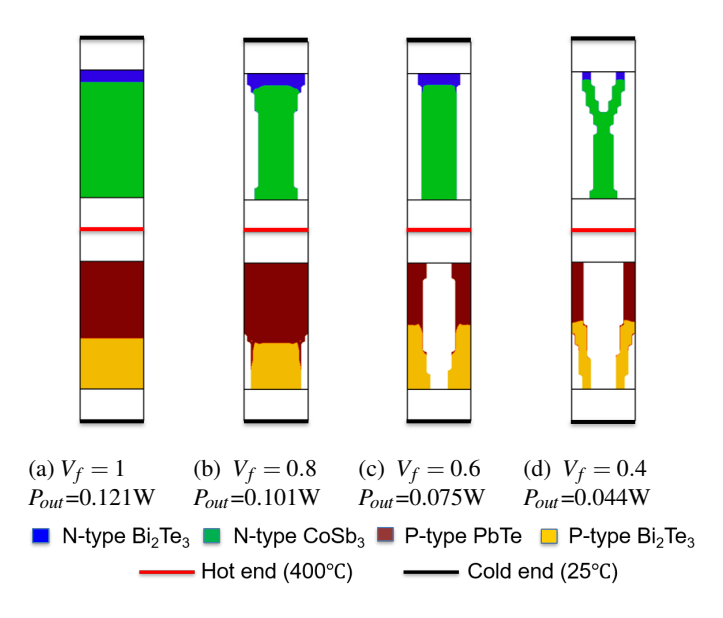


FIGURE 7: Different results for output power as the objective

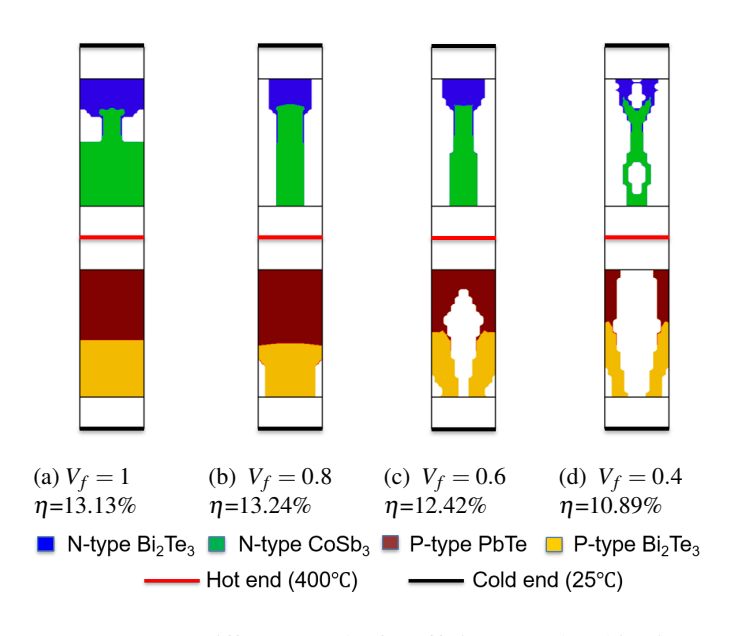


FIGURE 8: Different results for efficiency as the objective

tained from the subsequent 2.5D simulation are not that appealing, with each dropping nearly by 50%. This could be attributed to the following aspects.

First, for a certain layout of the TEG structure, the maximum output power, and conversion efficiency can be achieved when the external load value equals to or approach the internal electrical resistance of the TEG [25]. This means that the value of the external resistor needs to be updated in each iteration of the

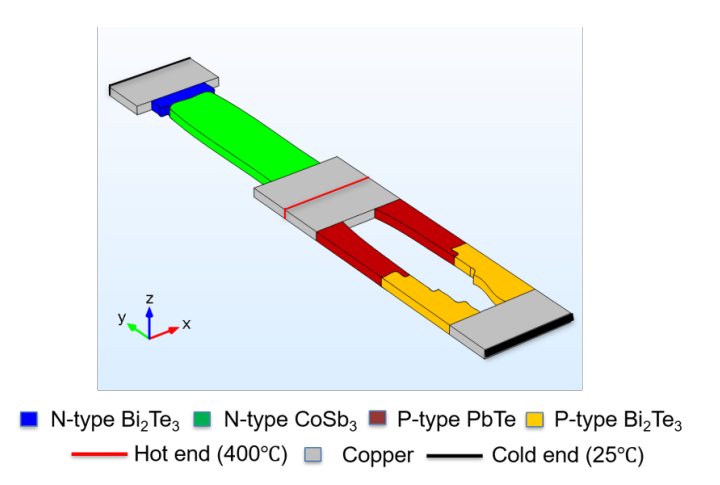


FIGURE 9: 2.5D model corresponding to $V_f = 0.6$ and output power as the objective

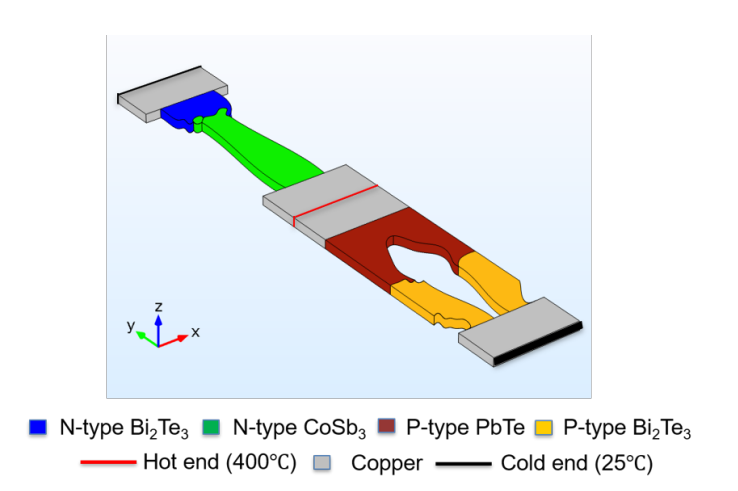


FIGURE 10: 2.5D model corresponding to $V_f = 0.6$ and conversion efficiency as the objective

topology optimization process to match that of the TEG functioning like a battery. But in this paper, the external load is kept as a constant for all different volume ratio conditions, which could leave some space for improvement of the two objective functions. Nevertheless, it still makes sense, for example, when you intend to optimize a TEG structure to charge a device whose electrical resistance is a constant. In the 2.5D simulation, however, the internal resistance of the TEG changes due to the removing of TE materials. As a consequence, the ratio between the fixed external load R and the internal resistance changes accordingly, resulting in a lower output power and conversion efficiency than expected. This argument can be favored by the fact that an optimal external load R can be found to achieve the highest value of the two objective functions as shown in Figure 15. The black dash line

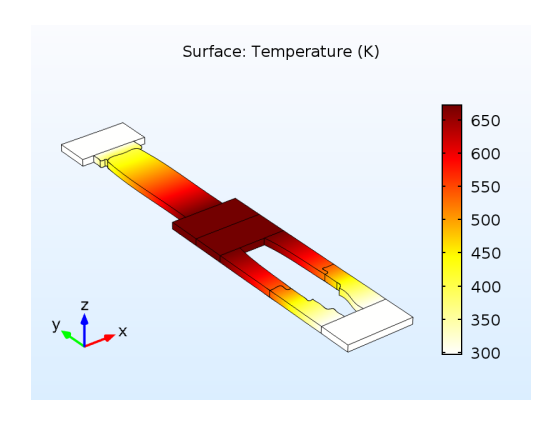


FIGURE 11: Temperature distribution corresponding to $V_f = 0.6$ and output power as the objective

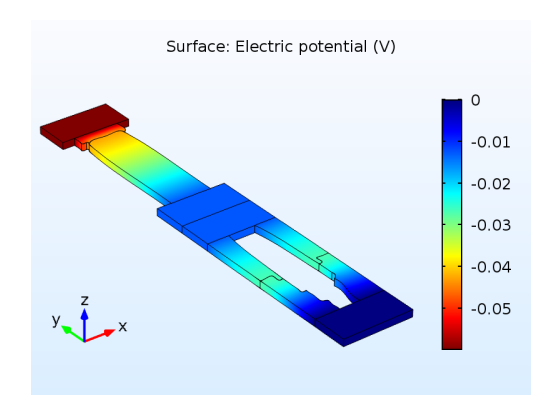


FIGURE 12: Electrical potential distribution corresponding to $V_f = 0.6$ and output power as the objective

corresponds to $R = 0.1\Omega$ as used in the 2.5D simulations.

Second and more important, as a common issue in SIMPbased topology optimization methods, there would exist a grey region representing the transition from one thermoelectric material to the other. Such a grey area corresponds to no physical material. One approach of getting rid of these transition zones is "power-law", in which a penalty factor is introduced in the interpolation scheme to penalize the intermediate density variables and force them to approach 0 or 1. In this paper, although the penalty factor p is set to be 3, the topology optimization results still show a quite large grey area. As shown in Figure 16, the surface for $\rho_1^p * \rho_2^p$ exhibits a quite large transition zone in the bottom P-type element (circled areas). The clear boundary between different thermoelectric materials can be obtained by setting up a threshold for ρ_1 and ρ_2 to distinguish one thermoelectric material from the other. However, this treatment would arouse another problem. The final designs are, to a certain degree, like segmented TEG. The performance of such structures depends not only on combining different thermoelectric materials but also on

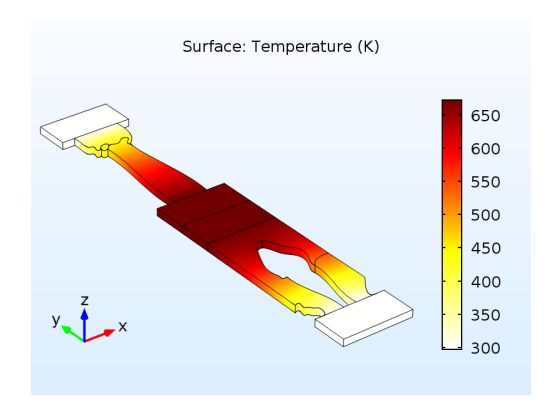


FIGURE 13: Temperature distribution corresponding to $V_f = 0.6$ and conversion efficiency as the objective

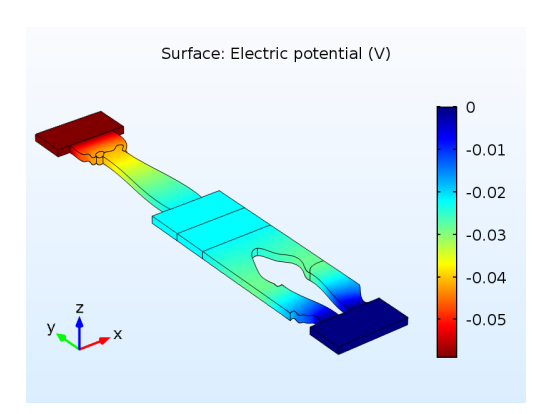


FIGURE 14: Electrical potential distribution corresponding to $V_f = 0.6$ and conversion efficiency as the objective

the compatibility factor. The compatibility factors must be close enough to ensure high conversion efficiency [26, 27, 28]. Thus, merely giving a threshold to separate one thermoelectric material from the other manually could yield a substantial difference in the compatibility factors and further low output power and conversion efficiency.

Based on the above discussion, several strategies may be adopted in the future to further improve current results: (1) include an inner optimization process to update the value of external load to match that of the TEG to ensure highest output power and conversion efficiency in each iteration; (2) try different interpolation scheme to reduce the grey region; (3) turn to alternative topology optimization methods, e.g. level-set method, which is known for its ability for making clear boundaries, to readdress this problem.

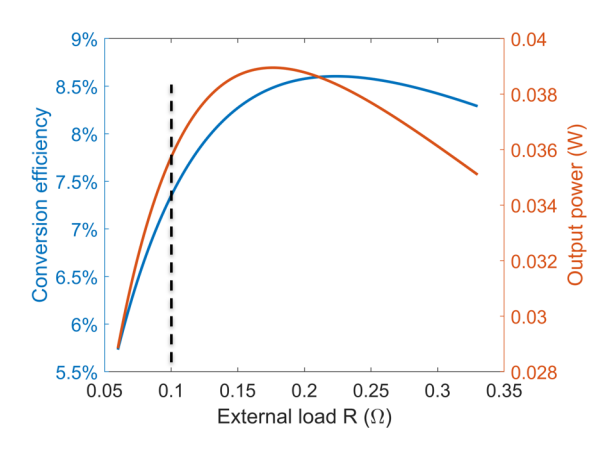


FIGURE 15: Conversion efficiency and output power as a function of external load *R* in the 2.5D simulations

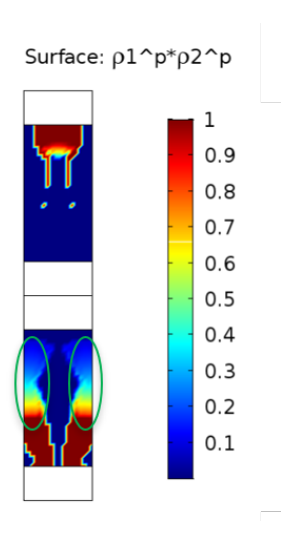


FIGURE 16: Grey region corresponding to $V_f = 0.6$ and conversion efficiency as the objective

ACKNOWLEDGMENT

The authors acknowledge the support from the National Science Foundation (Grants No. CMMI1462270, CMMI1762287, and ECCS1508862), Ford University Research Program (URP) (Award No. 2017-9198R), and the start-up grant from the State University of New York at Stony Brook.

REFERENCES

- [1] Snyder, G. J., and Toberer, E. S. "Complex thermoelectric materials". *Nature materials*, 7(2), p. 105.
- [2] Zhang, X., and Zhao, L.-D. "Thermoelectric materials: Energy conversion between heat and electricity". *Journal of Materiomics*, 1(2), pp. 92–105.

- [3] Zhao, L.-D., Lo, S.-H., Zhang, Y., Sun, H., Tan, G., Uher, C., Wolverton, C., Dravid, V. P., and Kanatzidis, M. G. "Ultralow thermal conductivity and high thermoelectric figure of merit in SnSe crystals". *Nature*, *508*(7496), p. 373.
- [4] Biswas, K., He, J., Blum, I. D., Wu, C.-I., Hogan, T. P., Seidman, D. N., Dravid, V. P., and Kanatzidis, M. G. "High-performance bulk thermoelectrics with all-scale hierarchical architectures". *Nature*, 489(7416), p. 414.
- [5] Hicks, L., and Dresselhaus, M. S. "Effect of quantum-well structures on the thermoelectric figure of merit". *Physical Review B*, *47*(19), p. 12727.
- [6] Pei, Y., Wang, H., and Snyder, G. J. "Band engineering of thermoelectric materials". *Advanced materials*, **24**(46), pp. 6125–6135.
- [7] He, J., Kanatzidis, M. G., and Dravid, V. P. "High performance bulk thermoelectrics via a panoscopic approach". *Materials Today*, *16*(5), pp. 166–176.
- [8] El-Genk, M. S., and Saber, H. H. "High efficiency segmented thermoelectric unicouple for operation between 973 and 300 K". *Energy Conversion and Management*, 44(7), pp. 1069–1088.
- [9] Bendsøe, M. P., and Kikuchi, N. "Generating optimal topologies in structural design using a homogenization method". Computer methods in applied mechanics and engineering, 71(2), pp. 197–224.
- [10] Bendsøe, M. P. "Optimal shape design as a material distribution problem". *Structural optimization*, 1(4), pp. 193–202.
- [11] Zhou, M., and Rozvany, G. "The COC algorithm, Part II: topological, geometrical and generalized shape optimization". *Computer Methods in Applied Mechanics and Engineering*, **89**(1-3), pp. 309–336.
- [12] Allaire, G., Jouve, F., and Toader, A.-M. "Structural optimization using sensitivity analysis and a level-set method". *Journal of computational physics*, *194*(1), pp. 363–393.
- [13] Wang, M. Y., Wang, X., and Guo, D. "A level set method for structural topology optimization". *Computer methods in applied mechanics and engineering*, **192**(1-2), pp. 227–246.
- [14] Bourdin, B., and Chambolle, A. "Design-dependent loads in topology optimization". *ESAIM: Control, Optimisation and Calculus of Variations*, **9**, pp. 19–48.
- [15] Sokolowski, J., and Zochowski, A. "On the topological derivative in shape optimization". *SIAM journal on control and optimization*, *37*(4), pp. 1251–1272.
- [16] Landau, L. D., Bell, J., Kearsley, M., Pitaevskii, L., Lifshitz, E., and Sykes, J., 2013. *Electrodynamics of continuous media*, Vol. 8. elsevier.
- [17] Takezawa, A., and Kitamura, M. "Geometrical design of thermoelectric generators based on topology optimization". *International Journal for Numerical Methods in Engineering*, **90**(11), pp. 1363–1392.

- [18] Bell, L. E. "Cooling, heating, generating power, and recovering waste heat with thermoelectric systems". *Science*, *321*(5895), pp. 1457–1461.
- [19] Bendsøe, M. P., and Sigmund, O. Topology optimization: theory, methods and applications. 2003.
- [20] Svanberg, K. "The method of moving asymptotesa new method for structural optimization". *International journal for numerical methods in engineering*, **24**(2), pp. 359–373.
- [21] Kajikawa, T., Rowe, D., and Rowe, D. "Thermoelectric handbook: macro to nano". *CRC/Taylor & Francis, Boca Raton, FL, USA*.
- [22] Heremans, J. P., Jovovic, V., Toberer, E. S., Saramat, A., Kurosaki, K., Charoenphakdee, A., Yamanaka, S., and Snyder, G. J. "Enhancement of thermoelectric efficiency in PbTe by distortion of the electronic density of states". *Sci*ence, 321(5888), pp. 554–557.
- [23] Zienkiewicz, O. C., Taylor, R. L., Zienkiewicz, O. C., and Taylor, R. L., 1977. *The finite element method*, Vol. 36. McGraw-hill London.
- [24] Allaire, G. "A review of adjoint methods for sensitivity analysis, uncertainty quantification and optimization in numerical codes". *Ingénieurs de l'Automobile*, **836**, pp. 33–36.
- [25] Goldsmid, H. J., 2010. *Introduction to thermoelectricity*, Vol. 121. Springer.
- [26] Wu, Y., Yang, J., Chen, S., and Zuo, L. "Thermo-element geometry optimization for high thermoelectric efficiency". *Energy*, *147*, pp. 672–680.
- [27] Snyder, G. J. "Application of the compatibility factor to the design of segmented and cascaded thermoelectric generators". *Applied physics letters*, **84**(13), pp. 2436–2438.
- [28] Hadjistassou, C., Kyriakides, E., and Georgiou, J. "Designing high efficiency segmented thermoelectric generators". *Energy conversion and management,* 66, pp. 165–172.